Operational research on a high-T_c rectifier-type superconducting flux pump

Jianzhao Geng, K. Matsuda, Lin Fu, Boyang Shen, Xiuchang Zhang, and T. A. Coombs

Department of Engineering, University of Cambridge, Cambridge, CB3 0FA, United Kingdom

Email: jg717@cam.ac.uk

High-T_c Superconducting (HTS) flux pumps are capable of injecting flux into a superconducting circuit, which can achieve persistent current operation for HTS magnets. In this paper, we studied the operation of a rectifier-type HTS flux pump. The flux pump employs a transformer to generate high alternating current in its secondary winding which is connected to an HTS load shorted by an HTS bridge. A high frequency AC field is intermittently applied perpendicular to the bridge, thus generating flux flow. The dynamic resistance caused by the flux flow "rectifies" the secondary current, resulting in a direct current in the load. We have found that the final load current can be easily controlled by changing the phase difference between the secondary current and bridge field. Bridge field of frequency ranging 10Hz-40Hz, magnitude ranging 0-0.66T was tested. Flux pumping was observed for field magnitude of 50mT or above. We have found that both higher field magnitude and higher field frequency result in a faster pumping speed and a higher final load current. This can be attributed to the influence of dynamic resistance. The dynamic resistance measured in the flux pump is comparable with the theoretical calculation. The experimental results fully support a first order circuit model. The flux pump is much more controllable than travelling wave flux pumps based on permanent magnets, which makes it promising for practical use.

1 Introduction

With the advancement in manufacturing Coated Conductor (CC) wires, CC coils are becoming ideal candidates for magnets, like in NMR [1], motor windings [2], et al. CC coils operating in persistent current mode can achieve better field stability and reduce power loss compared with being powered by current sources [3]. In practice, however, coils cannot work in real persistent current mode because of flux creep [4] and joint resistance [5]. Moreover, coils operating under a varying magnetic field suffer significant hysteresis loss. A rotor winding is a particular case, which suffers travelling magnetic fields generated by harmonics in the stator windings. Flux pumps can inject flux into superconducting circuits using external field, without electrical contact. They are competitive candidates for compensating the current decay in coils, thus making them work in real persistent current mode. LTS flux pumps [6, 7] have been studied for decades. Most of them can be described as rectifiers in circuit analogue. The key point in these flux pumps is to drive at least one part of superconductor normal either by high field or heat. Developed in recent years, HTS flux pumps [8-15] are mainly based on travelling magnetic waves, which was first proposed by Coombs [8]. Bai [9, 10] achieved flux pumping using travelling wave generated by

linear windings. Hoffman [11, 12] discovered that flux pumping can be achieved using magnets spinning across HTS tapes.

2 Flux pumping mechanism

In recent work [16], we proposed a new flux pumping mechanism which uses AC field triggered flux flow. As shown in Fig. 1(a), a transformer generates high alternating current i_P in its secondary winding, which is formed by a closed HTS tape and we call it "the charging loop", and i_P is called the charging current. A portion of the tape, which we refer to as "the bridge", shorts an HTS load, thus forming the load loop. Initially, the high alternating current only flows through the bridge (denoted by i_B) rather than through the HTS load, because there is nearly no resistance or inductance in the bridge. When an AC magnetic field B_{app} is applied perpendicular to the bridge tape surface, flux flows into the load through the bridge, thus generating a voltage across the bridge.

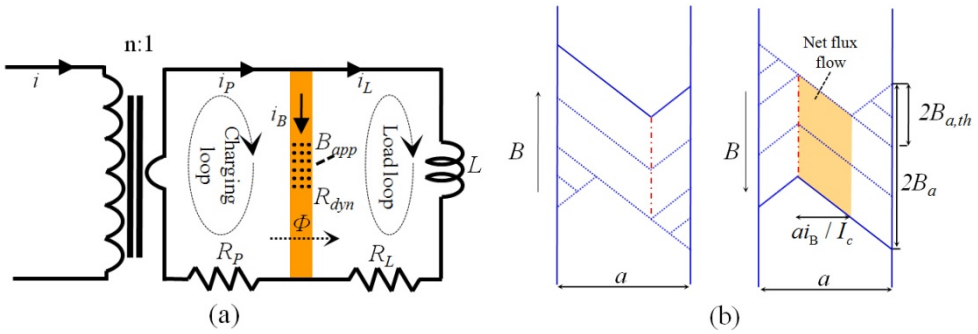

FIG. 1. Schematic drawing the proposed flux pump. (a) Circuit analogue. (b) Flux flow process in a DC carrying superconductor under perpendicular AC field [21, 22].

Fig. 1(b) shows the flux flow process of an infinitely thick superconductor carrying DC under AC field [17-22] under Bean's model [23]. The process is similar to a bridge with finite thickness. Assuming the superconductor with a width of a is carrying a current i_B which flows in the direction perpendicular to the paper. An AC field is applied perpendicular to the current direction. In the field rising process most flux enters the superconductor from its left edge, while in field falling process most flux leaves the superconductor from the right edge, as shown in Fig. 1(b). Therefore, there is hysteresis, and a net flux flows across the superconductor from left to right. The shaded area in Fig. 1(b) indicates the net flux flow per unit length (Wb/m) per cycle. For a tape with limited thickness, although the field profile is different from Fig. 1(b), the process is very similar when the field is high [24]. The total amount of flux which flows across the bridge superconductor per field cycle, therefore, can be described as:

$$\Delta\Phi = \frac{2ali_B}{I_c}(B_a - B_{a,th}) \quad (1)$$

Where l is the length of the tape subjected to the field, I_c is the tape critical current, B_a is the half peak-peak value of the applied field, and $B_{a,th}$ is the threshold field [18]. As can be seen from Eq. (1), the flux flow direction is only determined by the direction of transport current. Therefore, the flux flow effect can also be described as a dynamic resistance [20]:

$$R_{dyn}=\frac{2alf}{I_c}(B_a-B_{a,th}) \quad (2)$$

If the bridge field frequency is much higher than the charging current frequency, the current seen by the field is quasi-DC. If we intermittently apply the bridge field when the bridge current is in the same polarity, the flux flow effect can accumulate, thus resulting in flux pumping. Fig. 2 shows the waveform of charging current i_P, bridge field B_{app}, bridge current i_B and load current i_L under this scheme.

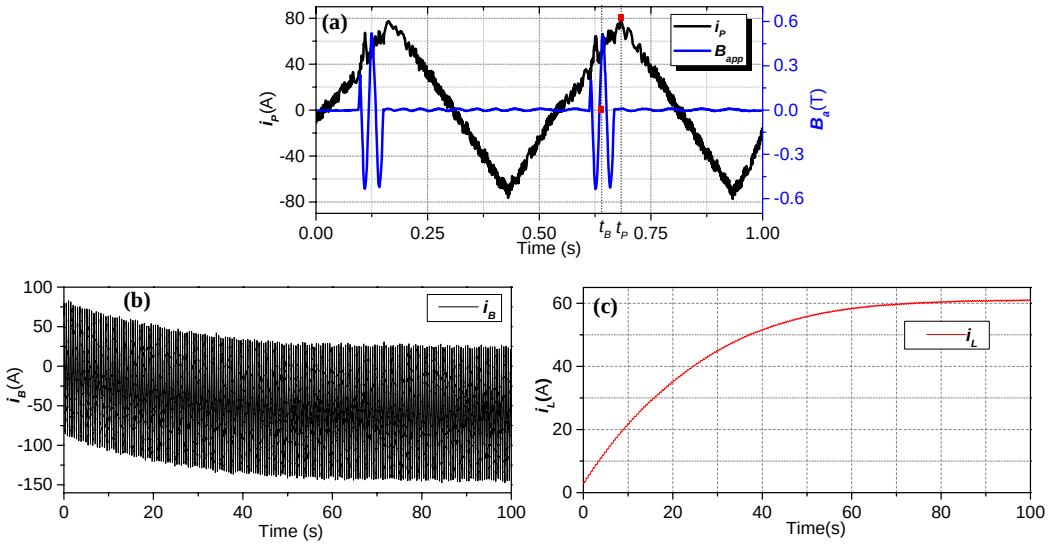

FIG. 2. Waveforms of bridge field and currents in the proposed flux pump. (a) Charging current i_P and bridge field B_{app}. t_B and t_P denotes the time center of B_{app} duration and i_P peak time respectively. (b) Bridge current i_B. (c) Load current i_L.

By assuming the bridge is a field controlled variable resistor, the flux pump acts like a rectifier. We developed an analytical solution for load current based on the circuit model in Fig. 1(a) [16]:

$$\begin{cases} i_L=A(1-e^{-t/\tau}) \\ A=I_P/(1+R_L/R_{dyn}p) \\ \tau=L/(R_L+R_{dyn}p) \end{cases} \quad (3)$$

Where

$$I_P=\frac{1}{pT}\int_{B_{app}\,\mathrm{on}} i_P dt \quad (4)$$

which describes the average charging current during the time bridge field is applied, p is the time proportion of field applied duration over charging current period T, R_L is the equivalent loss resistance in the load loop. As can be seen from Eq. (3), I_P only influences the final load current, while R_{dyn} and p influence both the pumping speed and final load current. According to Eq. (2) and Eq. (3), many factors, such as bridge field magnitude, frequency, duration, charging current magnitude, waveform, and relative phase between bridge field and charging current, will all influence the performance of the flux pump. Therefore, in the following part, we experimentally study the influence of each factor.

3 Experimental system

The experimental system is shown in Fig. 3. The whole superconducting circuit was formed by *Superpower* 6mm stabilized tape. The load double pancake coil had an inductance of 0.388mH and a critical current of 81A. The bridge superconductor, which has an effective length of 3.5cm was subjected to a perpendicular AC field generated by an electromagnet. The critical current of the bridge superconductor was measured to be 123A (with 1μV/cm criterion). Two power supplies were used in the experiment, one for the transformer, the other for the magnet. Synchronised signals generated by LabVIEW software and a DAC card were used to control the two power supplies. Load current i_L was measured by a Hall sensor fixed in the centre of the load, i_P was measured by an open loop Hall Effect current sensor, and B_{app} was monitored by measuring the current supplying the magnet. The superconducting circuit was cooled using liquid nitrogen.

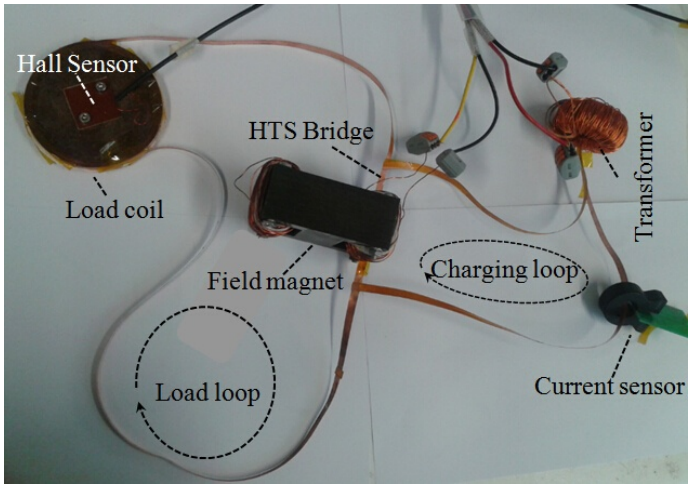

FIG. 3. Picture of the proposed flux pumping system.

4 Operation of the flux pump

In this part, we present the operational characteristics of the proposed flux pump. In the following experiment, the waveform of i_P is symmetrical triangular, the frequency of i_P is 2Hz, p is 0.1, B_{app} is applied around the positive peak of i_P, unless otherwise specified.

4.1 Influence of charging current magnitude on pumping performance

In the experiment of this section, the magnitude of charging current i_P was changed from 69A to 109A, with an increment of about 10A. Other parameters were fixed as: applied field magnitude 0.49T, applied field frequency 40Hz. Fig. 4(a) shows the load current waveform under different magnitude of i_P. The influence of i_P magnitude on flux pumping performance is quite complicated. In terms of pumping speed, the load current saturates faster with a higher i_P magnitude. The final load current, however, does not always increase with the increase of i_P magnitude. Maximum load current is achieved when the i_P magnitude is 80A. The final load current level decreases with the further increase of i_P magnitude.

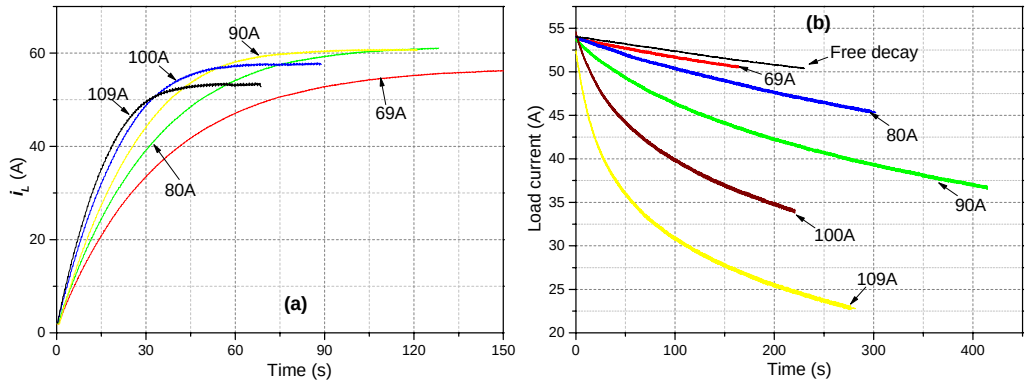

FIG. 4. Plots showing the load current curves under different charging current i_P. (a) Charging the load. (b) Decay result, after charging the load, the bridge field was turned off.

According to Eq. (3), the final load current should be proportional to the magnitude of i_P. However, Eq. (3) describes the ideal case without considering the current capacity of the bridge superconductor. Considering i_B=i_P-i_L, with the increase of i_L, i_B will reach a high value when i_P is around its negative peak, which can be seen from Fig. 2(b). The critical current of the bridge superconductor is only 123A, if the bridge current exceeds this value, a certain amount of current has to flow through the parallel copper layer, thus generating a loss (in Eq. (3), we treat this loss as one source of R_L). To study this loss, a decay experiment was conducted under different charging current magnitudes. In each case, the load current was firstly pumped up to saturated value, then the bridge field was switched off, but the charging current remained. To make a comparative study, a free decay experiment was also conducted, in which both of the applied field and the charging current were switched off after charging the load. Fig. 4(b) shows the load current decay curves. The plot begins with all currents decaying to about 54A. As shown in Fig. 4(b), in the free decay case, the load current decays slower than all of those with charging current, and the decay speed remains constant. The free decay is mainly caused by the joint resistance. For all cases with charging current, larger charging current magnitude causes a faster load current decay. For charging current magnitude of 80A or above, the load current decay rate is not constant. These load currents decay faster in the beginning, and gradually slow down. In the 69A charging current case, load current decays slightly slower than free decay case, with a nearly constant decay rate. The load current decay with charging current is mainly caused by the limitation of critical current of bridge superconductor.

In the charging up process, the load current saturates when the bridge field triggered flux flow is balanced by the flux consumption in the load loop which is contributed largely by the over current on the bridge, i. e.:

$$\Delta\phi_{\text{on}} = \int_{B_{app}\,\text{on}} (I_P - i_L) R_{dyn} dt = \Delta\phi_{\text{off}} \approx \int_{B_{app}\,\text{off}} v_B dt \quad (5)$$

Where v_B is the bridge voltage when field is off. For charging current magnitude of 80A case, the final I_P-i_L≈9A, and R_{dyn}≈0.13mΩ with 40Hz, 0.49T field. Considering p=0.1, $\Delta\phi_{\text{on}}$ is calculated to be 0.058mWb. Fig. 5 shows the V-I curve of a tape which has the same type and length as the bridge tape. According to the V-I curve and waveform of i_p, the last term in Eq. (5) is estimated to be 0.02mWb-0.04mWb (it is unlikely to accurately calculated the value, because the sharp V-I curve will significantly amplify any measurement error in the current.). The difference between these two terms can be attributed to extra losses contributed by joint resistance and hysteresis.

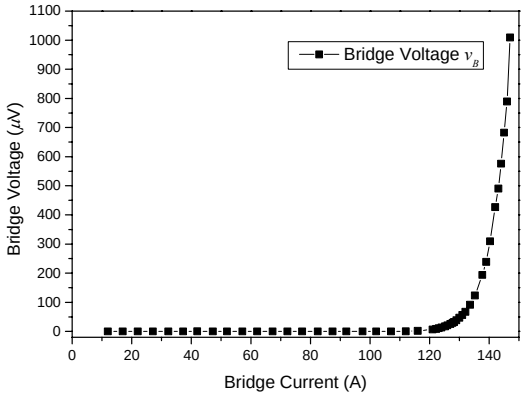

FIG. 5. V-I curve of a YBCO tape which has the same type and length as the bridge tape.

To overcome the current limit, one way could be increasing the width (current capacity) of the bridge. But in this way, the bridge field area and hence the inductance of the bridge magnet has to be increased to achieve the same dynamic resistance. An alternative solution is to generate an asymmetrical charging current, with its positive peak value larger than its negative peak value. The waveform is shown in Fig. 6(a), and the pumping result is shown in Fig. 6(b). It is clear that asymmetrical charging current results in a better performance compared with symmetrical one.

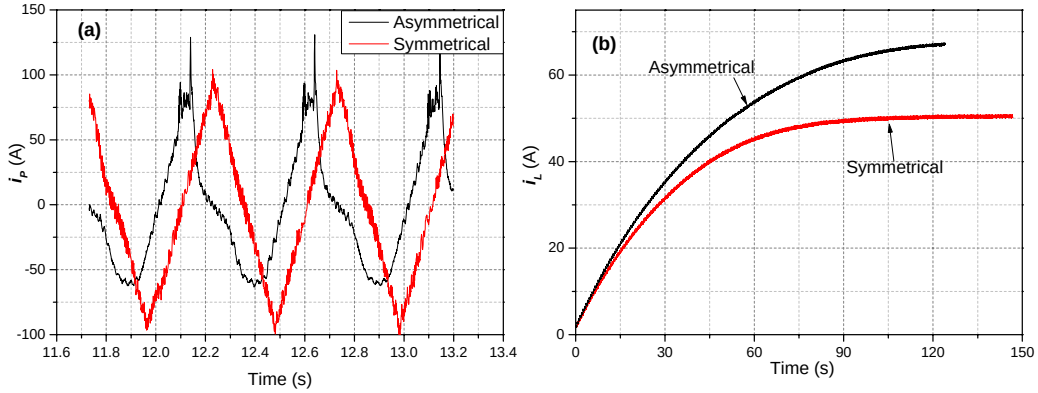

FIG. 6. Results on symmetrical and asymmetrical charging current experiment, where bridge field magnitude is 0.49T, frequency 20Hz. (a) Waveforms of charging current i_P. (b) Charging curve of load current i_L.

4.2 Influence of phase difference between transport current and bridge field on pumping performance

The phase difference between the applied field and transport current is defined as:

$$\Delta\theta=\frac{t_B-t_P}{T}\times 360^{\circ} \qquad (6)$$

Where t_B is the time centre of the applied field duration, t_P is positive peak time of i_P, and T is the period of i_P, as shown in Fig. 2(a). It should be noticed that we used a fixed time window pT to modulate B_{app}. If pT is not the integral multiples of B_{app} period, B_{app} has to be truncated. Therefore, $\Delta\theta$ relies on the centre of pT rather than the specific phase of B_{app}. If $\Delta\theta$=0°, it is defined as 'in phase'. The phase difference between transport current and applied field directly determines I_P. When $\Delta\theta$=0°, maximum I_P is achieved, whereas I_P=0 when $\Delta\theta$=90°. In the experiment of this section, all other parameters are fixed as: field frequency 30Hz, magnitude 0.49T, and charging current magnitude 77A.

Load current curves under different $\Delta\theta$ are shown in Fig. 7(a). Each waveform was then divided by its saturated value, and the result is shown in Fig. 7(b). As can be seen from Fig. 7, although the load current curves are different from one another in terms of magnitude, their time constants are very similar. This is because R_{dyn} is nearly independent of transport current when the applied field is high. The load current curve of $\Delta\theta$=0 saturated slightly faster than other cases, because the bridge current capacity limits the load current, as discussed above.

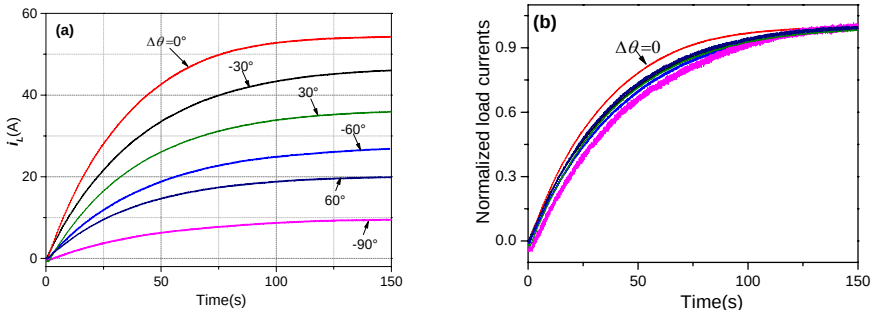

FIG. 7. Plots showing the load current curve under different values of $\Delta\theta$. (a) Load currents. (b) load currents divided by their final values.

Detailed experiments have also been done concerning the phase difference. We incremented the phase difference $\Delta\theta$ in 10° steps up to 180°. The result of I_P and final load current versus $\Delta\theta$ is shown in Fig. 8. The plot of I_P versus $\Delta\theta$ is similar as the time domain waveform of i_P. The maximum final load current is achieved when the applied field and the charging current are in phase. The curve is not perfectly symmetrical, mainly because of the distortion in the transport current, which can be partly seen in Fig. 6(a).

The results shown in this section indicate that the final load current can be easily controlled by changing the phase difference between bridge field and charging current. This is an obvious advantage over those travelling wave based flux pumps [8, 10].

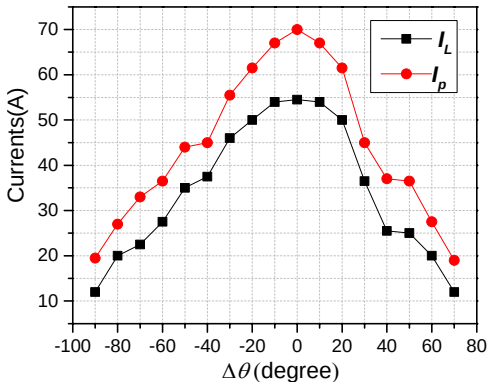

FIG. 8. Plots showing the final load current I_L and average charging current I_P over field duration with respect to $\Delta\theta$.

4.3 Influence of bridge field magnitude on pumping performance

The magnitude of applied field directly influences the amount of flux flowing across the bridge per cycle, as depicted in Fig. 1(b). It can also be considered as the influence on R_{dyn}, as described in Eq. (2). In this part of experiment, we tried to decrease the field magnitude from 0.66T to nearly zero, with all other parameters fixed as: magnitude of charging 90A, frequency of applied field 20Hz. The load current results under different field magnitudes are shown in Fig. 9.

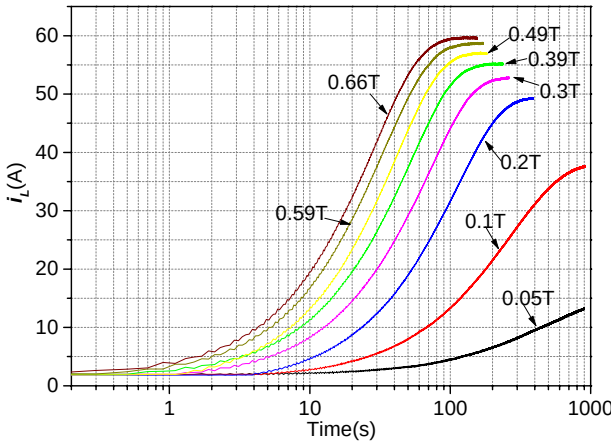

FIG. 9. Plots showing the waveform of load currents under different applied field magnitude. The field frequency is 20Hz.

As shown in Fig. 9, lager field magnitude generates a higher final load current level as well as a faster pumping speed. The minimum observable load current occurs when the field magnitude decreased to 50mT. In this case, it took about 15 minutes for the load current to saturate at about 13A. With field less than 50mT, no load current was observed, mainly because there was a noise of about 10mT in the field.

The load currents under B_a=0.65T and 50mT are shown in Fig. 10, together with a first order fitting.

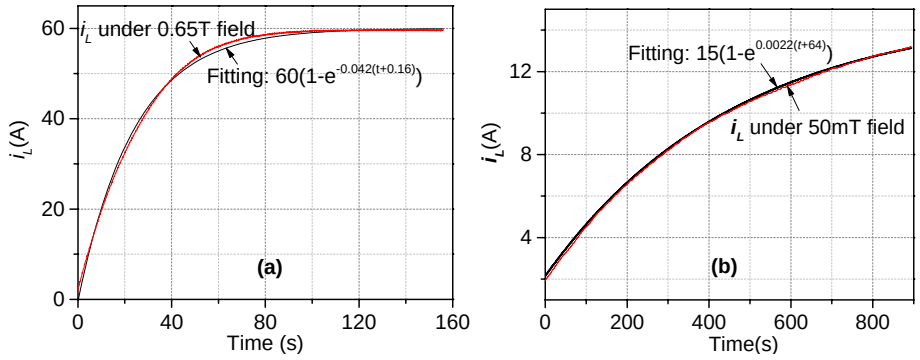

FIG. 10. Plots showing the load current curves and fitting curves. (a) under B_a=0.65T.(b) under B_a=50mT.

Each load current curve can be well fitted by a first order exponential fitting, which well proves the analytical model in Eq. (3). The fitting error in Fig. 10(a) is larger than that in Fig. 10(b). This is because for final load current less than 33A (123A-90A) the bridge current never exceeded the critical value of 123A, so R_L *is* nearly constant; whereas for final load more than 33A, the loss in the load loop (mainly on the bridge) increases with the increase of load current, resulting in a variable R_L. However, the error is tolerable by considering an averaged constant R_L.

The load current curve under 50mT field can be well fitted by:

$$i_L = 15\left(1 - e^{-0.0022(t+64)}\right) \qquad (7)$$

Considering the value of I_P is about 74A, from Eq. (3) and Eq. (7), we can calculate the value of the threshold field $B_{a,th}$ is around 25mT. The value is comparable with the measured value of 18mT under 60A DC current. All other load current curves can also be well fitted by a first order exponential fitting. The dynamic resistance values were calculated based on these fittings. The dynamic resistance are also calculated by Eq. (2), under Bean's model. Both results are shown in Fig. 11. The different between the measured value and predicted value under Bean's assumption is small when the field magnitude is less than 0.1T. And it increases with the increase of field magnitude. The result indicates a very strong field dependency of critical current density in the bridge superconductor.

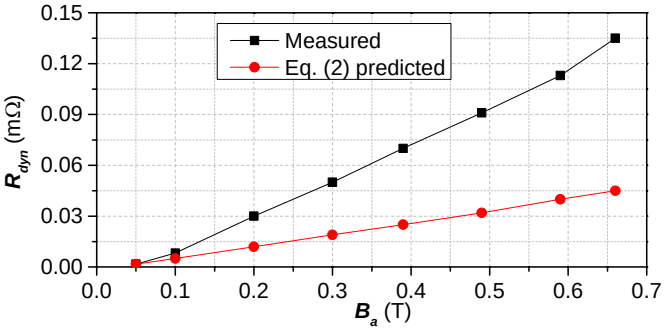

FIG. 11. Plots showing the calculated dynamic resistance under Bean's model and the measured value in the pump under different field magnitudes.

4.4 Influence of bridge field frequency on pumping performance

The magnitude of B_{app} influences the amount of flux flowing across the bridge per cycle, whereas the frequency of bridge field determines the number of cycles in a certain amount of time. Therefore, the total flux flow should be proportional to field frequency, which can also be seen from Eq. (2) in terms of dynamic resistance. In this part of experiment, all other parameters were fixed except the applied field frequency. The charging current magnitude was 90A, applied field magnitude was 0.49T. The frequency of applied field varied from 10Hz to 40Hz with a 10Hz increment. The load currents are shown in Fig. 12. The result shows that both of the pumping speed and final load current level can be enhanced by the increasing of bridge field frequency.

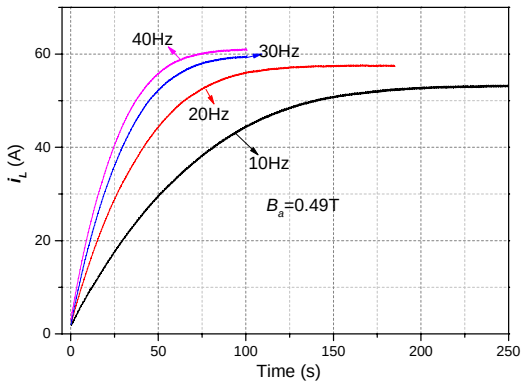

FIG. 12. Plots showing the load current curves under different applied field frequencies. The field magnitude is 0.49T.

The current curves are fitted by first order exponential equations. The values of dynamic resistance are calculated from the fitting and also from Eq. (2). The measured value of R_{dyn} is not strictly proportional to field frequency. This is mainly because our control strategy. During each charging current cycle, the field applied duration is fixed as 0.05s, which may truncate the field signal, so that transience is inevitable in the field. The transience will increase the actual field frequency. The effect is more significant when the field frequency is low, because fewer cycles of field are applied.

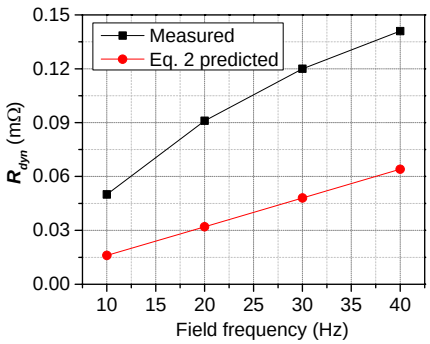

FIG. 13. Plots showing the calculated dynamic resistance under Bean's model and the measured value in the pump under different field frequencies.

4.5 Influence of charging current frequency on pumping performance

According to Eq. (3), the performance of the pump is independent of frequency of i_P, as long as p is fixed. Eq. (3) describes the ideal case, where the transformer is ideal. In practical, if the transport current frequency is too low, say less than 0.5 Hz, the iron core of the transformer is likely to saturate. In this case, the charging current can not remain controlled. In the following experiment, we choose to vary the frequency from 1.5Hz to 3Hz. Other parameters are: i_P magnitude 90A, applied field magnitude 0.49T, applied field frequency 40Hz.

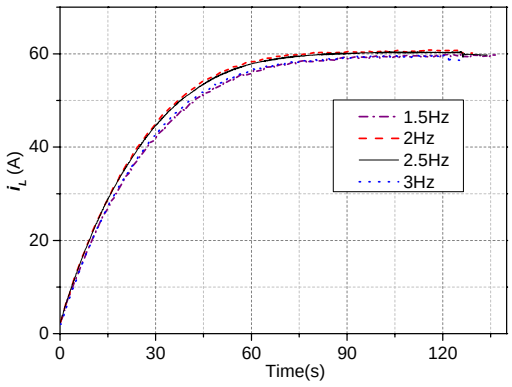

FIG. 14. Plots showing the load current curves under different charging current frequencies.

As shown in Fig. 14, there are very little differences between the four curves. The 1.5Hz and 3Hz curves are nearly overlapped, and the 2Hz and 2.5 Hz curves are nearly overlapped. A slight difference occurs between these two groups. This may be caused by some synchronising error between i_p and modulated B_{app} in 1.5 and 3Hz cases. Thus the pumping speed is slower and the final load current is smaller compared with 2Hz and 2.5 Hz cases. The experimental result verifies the prediction in Eq. (3) that transport current frequency has little influence on the pumping performance. In practical use, the transport current frequency should be as low as possible to reduce AC transport loss in the charging loop.

4.6 Influence of bridge field duration on pumping performance

The value of applied field duration p determines how long the field is applied in one charging current cycle. According to Eq. (3), a larger p means a faster pumping and a higher level of final load current. Rectangular charging current waveform was used in this section, so that I_P was independent of p. In theory, p can reach as high as 0.5. But in real experiment, the transformer was not powerful enough, so when p was larger than 0.3, the transport current was severely influenced by the load. The duration p, therefore, was chosen to vary from 0.1 to 0.25 to make sure that the transport current did not change too much. We can see from Fig. 15 that the final load current is positively correlated with p. When the load current is less than 30A, the pumping speed is nearly proportional to p, which well proves the model in Eq. (3).

In real application, a larger p is preferable. Because it can improve pumping performance without extra requirements on capacity of the power supplies. The advantage of using a rectangular charging current over a triangular one is that for rectangular wave I_P equals to the magnitude of i_P, so that we can achieve the same I_P with a relatively small i_P. The disadvantage is that we cannot flexibly control the load current level by changing the relative phase between the charging current and applied field.

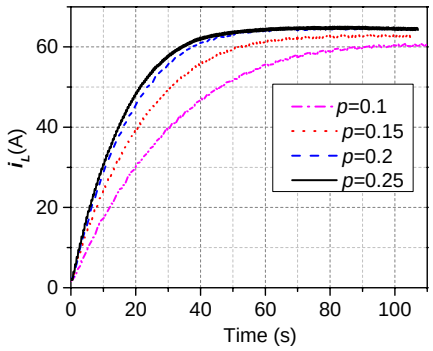

FIG. 15. Plots showing the load current curves under different time proportion of applied field.

5 Discussion

The proposed flux pump is superficially similar to LTS rectifier flux pumps from circuit point of view. However, their underlying physics are quite different. In LTS rectifier type flux pumps [6, 7], the bridge (or switch) is mainly controlled by intermittently driving the superconductor normal, using high field (either DC or DC biased AC) or heat. In this work, we use an AC field to control the bridge. The well known effect that flux flow can be triggered when a DC carrying type-II superconductor is subjected to a perpendicular AC field is used. The flux flow is achieved without driving the high-T_c superconductor either normal or into the flux flow region in E-J curve. There are two main drawbacks for using heat to drive a superconductor normal. One is that the heat control is slow, normally more than several seconds [25], which severely limits the operating frequency of the flux pump; the other is that any heat loss in a cryogenic system is undesirable. Using a high field to control an HTS switch is also undesirable because of the high critical field of high-T_c superconductors [26]. Using AC field instead can achieve a very fast control on the bridge. The dynamic resistance value is quite small. In the experiment, for example, it is normally less than 0.2mΩ. To increase the dynamic resistance, the either the field magnitude or field frequency has to be increased. This will be a challenge on power supply. Therefore, the flux pump is not suitable for charging a load with large inductance. However, it will be very promising to use this flux pumping method to operate large HTS loads in persistent current mode. It is very easy to achieve a joint with resistance less than 100nΩ, so the decay rate in HTS load is normally quite slow [27], which means a very small bridge resistance is enough to compensate the decay.

6 Conclusion

In this paper, we have presented the operational characteristics of an HTS transformer-rectifier type flux pump. The proposed flux pump is clear to understand and easily controllable. In the flux pump, a transformer was used to generate an alternating current with high magnitude and low frequency in its secondary winding. A load was connected across the secondary winding, and an AC magnetic field with high frequency was intermittently applied to an HTS bridge which shorted the secondary winding and the load. The AC field induced flux flow across the bridge, thus gradually charging the load. We experimentally examined the influential factors on the flux pump. These factors include charging current magnitude and waveform, bridge field magnitude, frequency and duration, phase difference between current and field. The flux pump is very easy to control. The pumping speed can be adjusted by changing the bridge field magnitude, frequency or duration. The final achievable load current can be controlled by changing charging current magnitude, bridge field, or their phase difference. All the result well validated our previously proposed analytic model. We have found that the dynamic resistance value in the pump is close to the prediction under Bean's assumption when the field magnitude is less than 0.1T, while it is two times larger when field magnitude reaches 0.66T. The result reflects a strong field dependency of critical current density. All the acquired operational characteristics are helpful for the optimization of flux pump. In future work, we will focus on the feedback control of the flux pump, through which we can automatically achieve a desirable load current level.

Acknowledgements

The authors would like to give sincere thanks to Mr. John Grundy for his help in the experiment. Jianzhao Geng would like to acknowledge Cambridge Trust for offering Cambridge International Scholarship to support his study in Cambridge.

References

[1] R. M. Walsh, R. Slade, D. Pooke, and C. Hoffmann, IEEE Trans. Appl. Supercond. **24**, 4600805 (2014).

[2] Y. Jiang, R. Pei, W. Xian, Z. Hong, and T A Coombs, Supercond. Sci. Technol. **21**, 065011 (2008).

[3] T. Tosaka, T. Kuriyama, M. Yamaji, K. Kuwano, M. Igarashi, and M. Terai, IEEE Trans. Appl. Supercond. **14**(2), 1218(2004).

[4] M. V. Feigel'man, V. B.Geshkenbein, and V. M. Vinokur, Phys. Rev. B **43**, 6263(R) (1991).

[5] Y. Kim, J. Bascuñán, T. Lecrevisse, S. Hahn, J. Voccio, D. Park, and Y. Iwasa, IEEE Trans. Appl. Supercond. **23**, 6800704 (2013).

[6] L. J. M. van de Klundert and H. H. J. ten Kate, Cryogenics **21**, 195 (1981).

[7] L. J. M. van de Klundert and H. H. J. ten Kate, Cryogenics **21**, 267 (1981).

[8] T. A. Coombs, GB2431519-A, 2007.

[9] Z. Bai, G. Yan, C. Wu, S. Ding, and C. Chen, Cryogenics **50**(10), 688 (2010).

[10] Z. Bai, C. Chen, Y. Wu, and Z. Zhen, Cryogenics **51**(9), 530 (2011).

[11] C. Hoffmann, D. Pooke, and A. D. Caplin, IEEE Trans. Appl. Supercond. **21**, 1628 (2011).

[12] C. Hoffmann, R. Walsh, E. Karrer-Mueller, and D. Pooke, Phys. Proc. **36**, 1324 (2012).

[13] W. Wang and T. A. Coombs, Supercond. Sci. Technol. **28**, 055003 (2015).

[14] L. Fu, K. Matsuda, M. Baghdadi, T. A. Coombs, IEEE Trans. Appl. Supercond. **25**, 4603804 (2015).

[15] Z. Jiang, C. W. Bumby, R. A. Badcock, H. Sung, N. J. Long and N. Amemiya, Supercond. Sci. Technol. **28**, 115008 (2015).

[16] J. Geng and T. A. Coombs, Appl. Phys. Lett. **107**, 142601 (2015).

[17] V. V. Andrianov, V. B. Zenkevich, V. V. Kurguzov, V. V. Sychev, and F.F. Ternovskii, Sov. Phys. JETP **31**, 815 (1970).

[18] T. Ogasawara, K. Yasukochi, S. Nose, and H. Sekizawa, Cryogenics **16**(1), 33 (1976).

[19] T. Ogasawara, Y. Takahashi, K. Kanbara, Y. Kubota, K. Yasohama, and K. Yasukochi, Cryogenics **19**(12), 736 (1979).

[20] M. P. Oomen, J. Rieger, M. Leghissa, B. ten Haken, and H. H. J. ten Kate, Supercond. Sci. Technol. **12**, 382 (1999).

[21] G. P. Mikitik and E. H. Brandt, Phys. Rew. B **64**, 092502 (2001).

[22] A. Uksusman, Y. Wolfus, A. Friedman, A. Shaulov, and Y. Yeshurun, J. Appl. Phys. **105**, 093921 (2009).

[23] C. P. Bean, Rev. Mod. Phys. **36**(1P1), 31 (1964).

[24] Y. Mawatari, IEEE Trans. Appl. Supercond. **7**, 1216 (1997).

[25] K.Koyanagi, S. Matsumoto, K. Fukushima, T. Kiyoshi, and H. Wada, IEEE Trans. Appl. Supercond. **12**, 7346962 (2002).

[26] Y. Iwasa, Cryogenics **43**, 303 (2003).

[27] T. Tosaka, et al., IEEE Trans. Appl. Supercond. **15**(2), 2293 (2005).